High-Bandwidth Current Control for Torque-Ripple Compensation in PM Synchronous Machines

Lothar Springob and Joachim Holtz, *Fellow, IEEE*

***Abstract*— Active compensation of torque harmonics in high-performance synchronous permanent magnet (PM) motor drives requires high-bandwidth current control. It is demonstrated that proportional integral (PI) current control exhibits performance limits, even when feedforward compensation of the rotor induced voltage and the stator inductance drop is used. High bandwidth requirements are satisfied using a digital deadbeat current controller. Sampling time delays are eliminated to the extent possible by means of a current predictor. The current controller and the predictor refer to a model of the parasitic effects of the PM synchronous machine that is acquired and adapted to parameter changes in real time. Stator current distortions due to deviations from the sinusoidal flux linkage distribution are thus eliminated. The control system facilitates compensation of high-frequency torque ripple of the machine.**

***Index Terms*— Current control, deadbeat control, estimation, permanent magnet motors, prediction, torque ripple.**

I. Introduction

PERMANENT MAGNET (PM) synchronous motors are used with preference for applications in high-performance positioning systems and machine tool spindle drives. Such servo drives must exhibit special characteristics. Apart from fast dynamic torque response, features like low torque ripple, high overload capability and operation in a wide speed range carry importance. A key element to achieve these goals is the current control and pulsewidth modulation scheme.

A preferred approach for fast current control is space-vector modulation with the fundamental current feedback signal being obtained by synchronized current sampling [1]. The maximum fundamental machine voltage can be increased by overmodulation techniques [2].

Torque ripple is reduced, but not eliminated, by appropriate magnetic design of the PM machine and by the layout of the stator winding [31]. Residual torque harmonics have been compensated by generating an inverse torque component through the q component of the stator current [4]–[7]. High-bandwidth current controllers are required for the practical implementation of harmonic torque compensation schemes, as the torque harmonic frequencies increase proportional to the rotor speed. Only at higher speed values is the effect of torque harmonics on the rotor speed reduced by the rotor inertia. Conventional PI controllers may exhibit bandwidth limits and are not suited to cover the full critical range of torque-ripple frequencies.

This paper presents a high-bandwidth current controller that solves the compensation problem by means of a deadbeat strategy. The approach can also be used for other, more general, current control applications. The controller is implemented in low-cost digital hardware. It comprises an adaptive machine model to describe the parasitic effects.

Manuscript received September 27, 1997; revised June 1, 1998. Abstract published on the Internet July 3, 1998.

L. Springob is with Vectron Elektronik GmbH, 47807 Krefeld, Germany.

J. Holtz is with the Electrical Machines and Drives Laboratory, Wuppertal University, 42097 Wuppertal, Germany.

Publisher Item Identifier S 0278-0046(98)07017-8.

II. Dynamic Model of a PM Machine

A. The Fundamental Machine

The dynamic representation of the PM machine is based on complex state variables [8]. Space harmonics and torque ripple induced by the rotor slots are neglected in a first approach and, hence, the analysis starts from the fundamental machine model. The voltage equation in a rotor-fixed reference frame (superscript $^{(R)}$) is

$$\boldsymbol{u}_s^{(R)} = r_s \boldsymbol{i}_s^{(R)} + \boldsymbol{l}_s^{(R)} * \frac{d\boldsymbol{i}_s^{(R)}}{dt} + j\omega \boldsymbol{l}_s * \boldsymbol{i}_s^{(R)} + \boldsymbol{u}_{i1}^{(R)} \qquad (1)$$

where $\boldsymbol{u}_s$ is the stator voltage, $\boldsymbol{i}_s$ is the stator current, r_s is the winding resistance, $\boldsymbol{u}_{i1}$ is the fundamental back EMF, and ω is the angular mechanical velocity of the rotor. The multiplication symbol $*$ is used in those equations in which a tensor multiplies with a space vector. Such product yields a space vector that differs from the original space vector, both in magnitude and in phase angle. All quantities are normalized by their rated values. Note that time is also normalized, $\tau = \omega_{sR} t$ [8], where ω_{sR} is the nominal stator frequency.

The magnetic saliency of the machines is expressed in (1) by the inductance tensor

$$\boldsymbol{l}_s^{(R)} = \begin{bmatrix} l_d & 0 \\ 0 & l_q \end{bmatrix}. \qquad (2)$$

The inductance tensor depends on the respective coordinate system [7]. It assumes its simplest mathematical form in rotor coordinates, being then independent of the rotor position angle δ. The following analysis is, therefore, restricted to rotor coordinates, and the superscript $^{(R)}$ is subsequently omitted for simplicity.

The inductance tensor expresses the fact that the flux linkage component of the stator winding $\boldsymbol{\psi}_s = \boldsymbol{l}_s * \boldsymbol{i}_s$, and the stator current $\boldsymbol{i}_s$ that produces this flux linkage component, have a

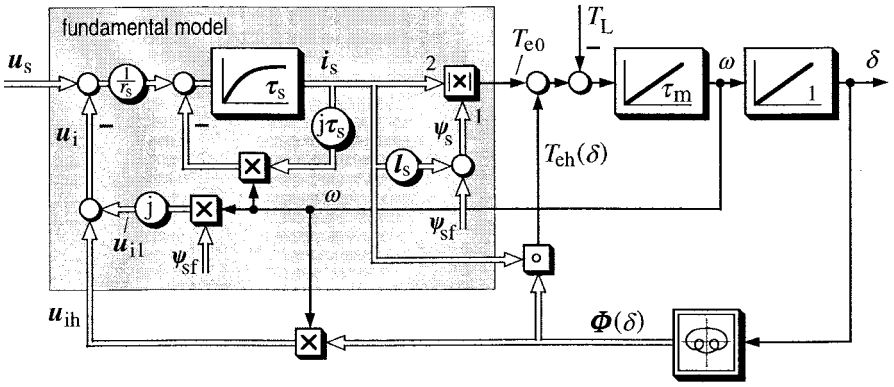

Fig. 1. Complex signal flow graph of a PM synchronous machine. The factor j advances a complex vector by $\pi/2$ in space.

phase displacement between them. The total stator flux linkage

$$\boldsymbol{\psi}_s(\delta) = \boldsymbol{l}_s(\delta) * \boldsymbol{i}_s + \boldsymbol{\psi}_{sf}(\delta) \tag{3}$$

has an added component $\boldsymbol{\psi}_{sf}$ that is owed to the fundamental flux linkage contribution of the permanent magnets in the rotor. Hence, the rotor induced voltage component in the stator is

$$\boldsymbol{u}_{i1} = j\omega\boldsymbol{\psi}_{sf}. \tag{4}$$

Dividing (1) by r_s yields

$$\boldsymbol{\tau}_s * \frac{d\boldsymbol{i}_s}{dt} + \boldsymbol{i}_s = -j\omega\boldsymbol{\tau}_s * \boldsymbol{i}_s + \frac{1}{r_s}(\boldsymbol{u}_s - \boldsymbol{u}_i) \tag{5}$$

where also the time constant $\boldsymbol{\tau}_s = \boldsymbol{l}_s/r_s$ enters as a tensor, which reflects that the rate of change of the d-axis current is different from that of the q-axis current, since $l_d \neq l_q$.

The fundamental electromagnetic torque T_{e0} is computed as

$$T_{e0} = \boldsymbol{\psi}_s \times \boldsymbol{i}_s\big|_z = (\boldsymbol{l}_s * \boldsymbol{i}_s + \boldsymbol{\psi}_{sf}) \times \boldsymbol{i}_s\big|_z. \tag{6}$$

The notation implies that only the z-component of the vector product is taken.

Based on (2)–(6), the fundamental PM machine is visualized in the upper left portion of the signal flow graph of Fig. 1 as a first-order system of the complex state variable $\boldsymbol{i}_s$.

B. Flux Linkage Harmonics

Although designed for sinusoidal flux linkage distribution, a real PM machine exhibits deviations from this ideal distribution. A torque ripple is generated in consequence, and an added harmonic component $\boldsymbol{u}_{ih}$ in the rotor induced stator voltage (4):

$$\boldsymbol{u}_i = \boldsymbol{u}_{i1} + \boldsymbol{u}_{ih} = j\omega\boldsymbol{\psi}_{sf} + \omega\frac{d\boldsymbol{\psi}_{sf}(\delta)}{d\delta}. \tag{7}$$

The factor

$$\frac{d\boldsymbol{\psi}_{sf}(\delta)}{d\delta} = \boldsymbol{\phi}(\delta) \tag{8}$$

in the added term expresses the change of stator flux linkage with the rotor position angle δ. According to (7), its effect on the rotor induced voltage increases as ω increases [7].

The two components of the rotor induced stator voltage (7) are displayed in Fig. 2. This oscillogram was obtained by measurement. Here, the fundamental component $\boldsymbol{u}_{i1}$ is fixed in space and aligned with the q-axis, while the harmonic component $\boldsymbol{u}_{ih}$ produces a closed trajectory which circles periodically around the tip of the space vector $\boldsymbol{u}_{i1}$. Since the harmonic trajectory almost overlaps itself in the course of a full rotor revolution, it is separately displayed for $\delta = 0 \cdots 180°$ in Fig. 2(a), and for $\delta = 180° \cdots 360°$ in Fig. 2(b). The oscillograms were recorded from an eight-pole PM machine, the data of which are listed in the Appendix. Note that all oscillograms in this paper are experimentally measured from a positioning servo system using that machine.

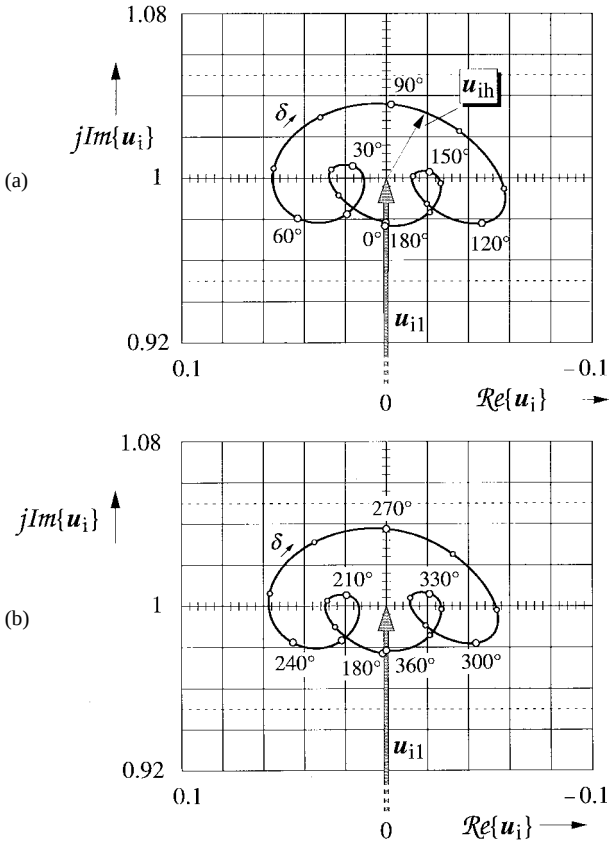

Fig. 2. Complex function $\boldsymbol{\Phi}(\delta)$ of the flux linkage harmonics. (a) During a first half revolution of the motor shaft $\delta = 0 \cdots 180°$. (b) During a second half revolution $\delta = 180° \cdots 360°$ The curves were obtained by measurement.

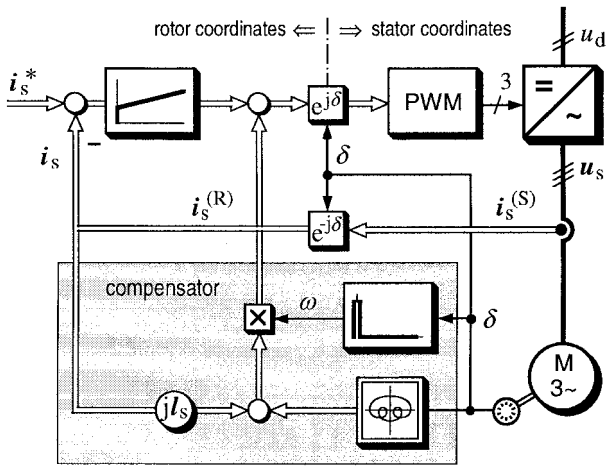

Fig. 3. Signal flow graph of a high-performance PI current controller; the shaded area highlights the feedforward compensator.

The harmonic torque is obtained from the equivalence of mechanical and electrical power, $\omega T_{eh} = \boldsymbol{u}_{ih}\boldsymbol{i}_s$, from which

$$T_{ch} = \frac{\boldsymbol{u}_{ih} \circ \boldsymbol{i}_s}{\omega} = \boldsymbol{i}_s \circ \frac{d\boldsymbol{\psi}_{sf}(\delta)}{d\delta} \tag{9}$$

is derived with reference to (7). The mechanical system is described by

$$\frac{d\omega}{d\tau} = \frac{1}{\tau_m}\left[T_{e0}(\tau) + T_{eh}(\delta) - T_L(\tau)\right] \tag{10}$$

and

$$\frac{d\delta}{d\tau} = \omega \tag{11}$$

where τ_m is the mechanical time constant, and T_L is the load torque.

Equations (7)–(11) are used to complete the signal flow graph of Fig. 1, which now includes the harmonic properties of a PM synchronous machine.

III. PI Current Control

The standard implementation of a digital PI current controller with synchronous fundamental current sampling [9] is shown in the upper portion of the signal flow graph of Fig. 3; it does not comprise the feedforward compensation that is marked by the shaded area below. A measured response of the current components i_d and i_q is displayed in Fig. 4(a). The test conditions are a step change of the current reference i_q^* at rated speed $\omega = -1$, where the superscript * marks a reference value. The following can be observed.

- Owing to the cross-coupling term $j\omega\boldsymbol{l} * \boldsymbol{i}_s$ in the system equation (1), the direct axis current i_d gets affected by the i_q command, which is undesired.
- A high-frequency ripple content is seen in both current components. It is mainly caused by the harmonic component $\boldsymbol{u}_{ih}$ of the rotor induced voltage. It causes a ripple component in the q-axis current, which increases the torque ripple.
- At no load, the i_q ripple was measured as $\pm 5\%$ and the i_q ripple as $\pm 8\%$. The current ripple increases as the load increases, owing to the mutual coupling of the current components; the i_q ripple is $\pm 8\%$ at rated load, and the i_d-ripple is $\pm 9\%$. The respective current components at rated load are shown in Fig. 4(b).

It is known that a feedforward compensation of the rotor induced voltage and the cross-coupling term improves the dynamic performance of the current control system. It eliminates the dynamic influence of the mechanical system and the load.

The compensations are highlighted by the shaded area in Fig. 3. An additional compensating term adds the harmonic components $\boldsymbol{u}_{ih}$ of the rotor induced voltage, which is the second term in (7).

The resulting step response is shown in Fig. 4(c). Cross coupling between the two axes is reduced. Owing to the harmonic feedforward term, the inverter output voltage and the rotor induced stator voltage of the machine have the same ripple content. This reduces the current ripple and, consequently, the torque ripple. The enlarged steady-state current waveform is shown in Fig. 4(d). Employing feedforward compensation changes the system dynamics and leads to different controller parameters. Thus, the response time of the current control is reduced. The controller is not fast enough, though, for active torque-ripple compensation.

IV. Deadbeat Current Control

Since the frequency of the harmonic torque components increases with speed, the efficient compensation by a counteracting electromagnetic torque requires a high-bandwidth current control system. Digital signal processing limits the achievable bandwidth owing to the inherent signal delay. The combination of a deadbeat current controller and a current predictor appears an appropriate approach to solve this problem.

The space-vector notation [5] will be used for the controller design, as it corresponds to the representation of the machine model [7] used in Fig. 1. The notation has been found expedient for the dynamic analysis of ac drive systems [10].

A. Principle of Deadbeat Current Control

Ideally, a deadbeat controller would establish zero current error within one sampling interval T_s. In a digital control system, the controller algorithm computes the required stator voltage vector such that the stator current error $\Delta\boldsymbol{i}_{s,k} = \boldsymbol{i}_{s,k}^* - \boldsymbol{i}_{s,k}$ at sampling instant k is eliminated in the next sampling instant, $\Delta\boldsymbol{i}_{s,k+1} = 0$. Referring to (1), (4), and (7), the required stator voltage at any next sampling instant $k+1$ is

$$\boldsymbol{u}_{s,k+1}^* = r_s\boldsymbol{i}_{s,k} + \boldsymbol{l}_s * \frac{\boldsymbol{i}_{s,k}^* - \boldsymbol{i}_{s,k}}{T_s} + j\omega\boldsymbol{l}_s * \boldsymbol{i}_{s,k} + \boldsymbol{u}_{i,k}(\delta) \tag{12}$$

which is the defining equation of the deadbeat controller. To verify (12), it is assumed that there is no change of current commanded at sampling instant k, $\boldsymbol{i}_{s,k}^* - \boldsymbol{i}_{s,k} = 0$. Then, the reference voltage need not change in the next

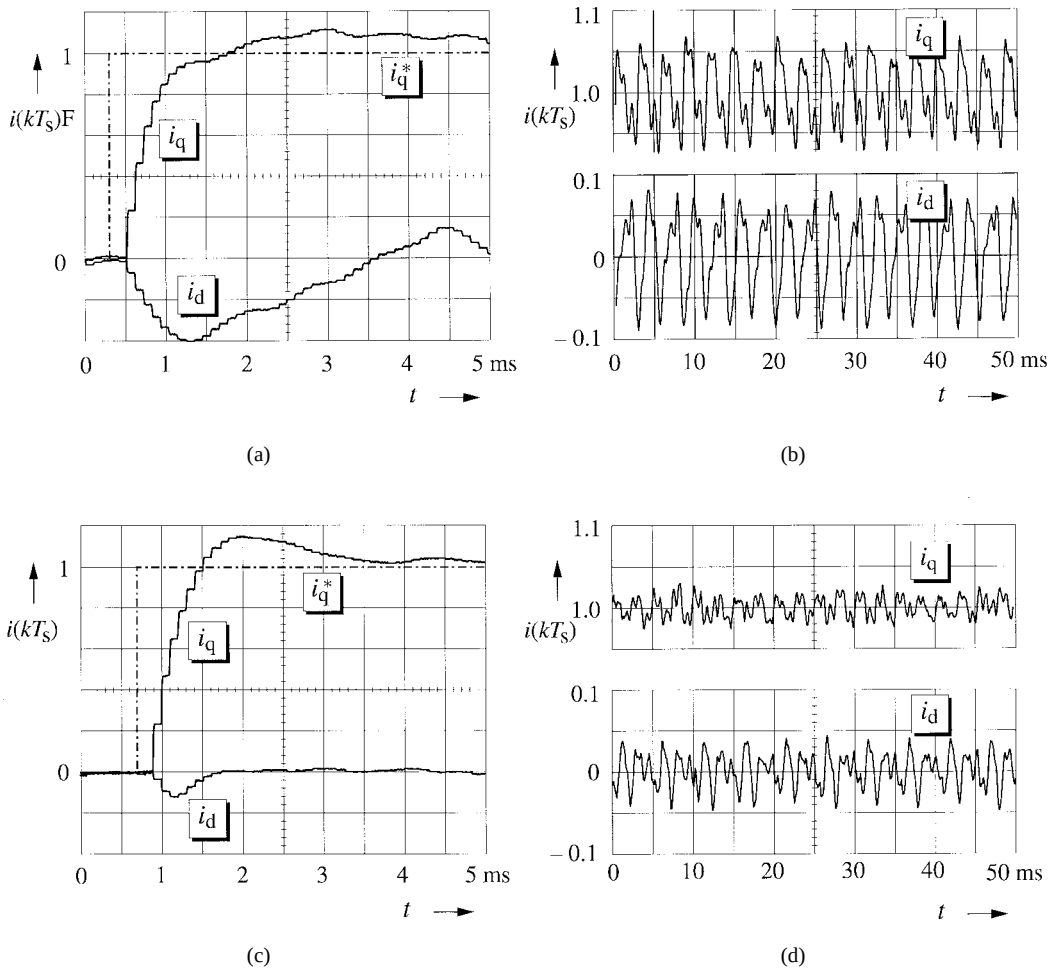

Fig. 4. Performance of a current-controlled space-vector modulator at regeneration $\omega = -1$. Upper line: without feedforward compensation. (a) Step response. (b) Steady-state current ripple at rated load (enlarged). Lower line: with feedforward compensation of fundamental current and torque ripple signal. (c) Step response. (d) Steady-state current ripple at rated load.

sampling instant, $\boldsymbol{u}^*_{s,k+1} = \boldsymbol{u}^*_{s,k}$, since $\boldsymbol{u}_{i,k}(\delta)$ is constant in rotor coordinates. Alternatively, a change of reference voltage $\boldsymbol{u}^*_{s,k+1} = \boldsymbol{u}^*_{s,k} + \boldsymbol{l}_s * \Delta\boldsymbol{i}_s/T_s$ effects a current change of exactly $\Delta\boldsymbol{i}_s$ for the next sampling instant.

The variables on the right-hand side of (12) are acquired at sampling instant k. The evaluation of (12) takes one sampling interval of duration T_s and, hence, the stator voltage command is available at the beginning of the $(k+1)$th sampling interval. Accordingly, the step response (Fig. 5) of the current loop exhibits a persistent oscillation which is caused by the time delay in (12).

The signal delay problem is overcome using a current predictor.

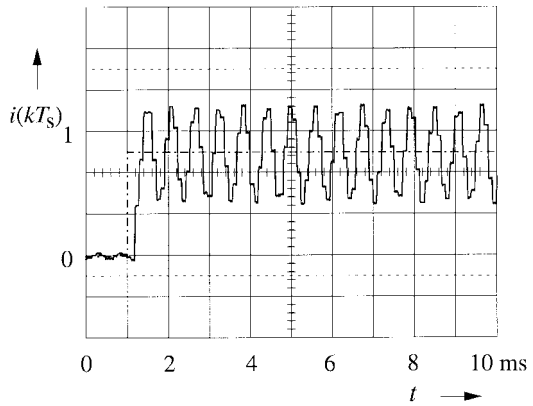

Fig. 5. Step response of a primitive deadbeat current controller.

B. Current Predictor

To eliminate the time delay in (12), the system state variables are required one sampling interval ahead in time. The predicted current is computed with reference to (1) as

$$\hat{\boldsymbol{i}}_{s,k+1} = \boldsymbol{i}_{s,k} + (\hat{\boldsymbol{u}}_{s,k} - r_s\boldsymbol{i}_{s,k} - \boldsymbol{u}_i(\delta)_k - j\omega\boldsymbol{l}_s * \boldsymbol{i}_{s,k})T_s * \boldsymbol{l}_s^{-1} \quad (13)$$

to replace the value $\boldsymbol{i}_{s,k}$ in (12):

$$\boldsymbol{u}^*_{s,k+1} = r_s\hat{\boldsymbol{i}}_{s,k+1} + \boldsymbol{l}_s * \frac{\boldsymbol{i}^*_{s,k} - \hat{\boldsymbol{i}}_{s,k+1}}{T_s} + j\omega_k\boldsymbol{l}_s * \hat{\boldsymbol{i}}_{s,k+1} + \boldsymbol{u}_i(\delta + \omega_k T_s). \quad (14)$$

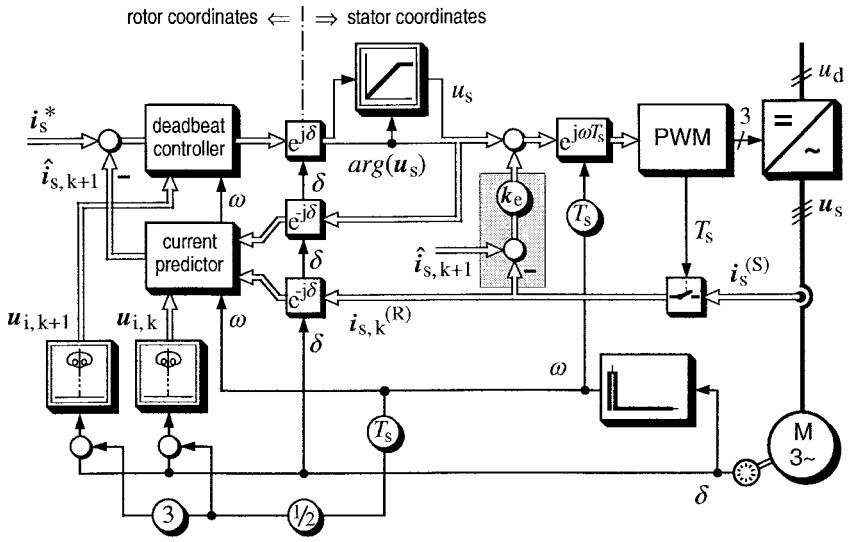

Fig. 6. Deadbeat current controller with current predictor. Signal flow graph (the shaded area marks the eddy current compensator).

Also, the total rotor induced voltage as defined by (7) is taken one sampling interval T_s ahead in time. The signal is read from a memory table with an angular displacement $\omega_k T_s$ as $\boldsymbol{u}_i(\delta)_{k+1} = \boldsymbol{u}_i(\delta + \omega_k T_s)$, where ω_k is the angular rotor frequency at sampling instant k.

Equation (14) defines a predictive deadbeat current controller. An overview of the resulting current control structure is shown in Fig. 6.

The numerical evaluation of the current predictor is sensitive to errors, as the voltage term on the right-hand side of (13) is computed as the difference of large quantities. It must be ensured in particular that the voltage $\hat{\boldsymbol{u}}_{s,k}$ in (13) is an exact prediction of the stator voltage $\boldsymbol{u}_{s,k}$ that is already being applied to the machine while (14) is numerically evaluated. Estimated or predicted values are marked by " $\hat{}$ ".

Prediction errors may be due to the following.

- The switching deadtime of the power switches produces a voltage error. The error must be eliminated using a suitable compensation technique [11].
- Another parasitic voltage component is introduced when torque ripple exists. This voltage appears as $\boldsymbol{u}_{ih}$ in (7). Its influence is compensated both in the deadbeat controller and the current predictor using the nonlinear functions $\boldsymbol{u}_i(\delta)$ shown in the lower left of Fig. 6. These functions are identified and adapted to parameter changes in real time, as reported in [7]. Modeling errors are minimum in this compensation, as the on-line adaptation scheme is fast and accurate.

  The same compensation is also used along with the PI controller in Fig. 3, and its effect is demonstrated in the oscillogram in Fig. 4(c).
- During large-signal transients, the deadbeat algorithm may calculate reference voltage vectors of high amplitude. The pulsewidth modulator then saturates, since the dc-link voltage is limited. It is this limited voltage vector which must enter as $\hat{\boldsymbol{u}}_{s,k}$ in (13). Its value should not be measured, if possible, as the additional hardware is normally not available. The magnitude of the limited stator voltage is estimated instead.

  The limit value is not constant, since the location of the voltage vector is restricted to a hexagonal area [9] and, hence,

$$u_{s\max} = \frac{\pi}{2\sqrt{3}\sin\left(\arg(u^*) - (n-1)\,\frac{\pi}{3} + \frac{\pi}{3}\right)}, \quad n \in 1, \cdots, 6 \tag{15}$$

  where n indicates the respective edge of the hexagon. The nonlinear reference voltage limiter is incorporated in the signal flow structure Fig. 6. The principle of voltage limiting is visualized in Fig. 7. The function (15) is read from a table when implemented in a microcontroller.

  Very favorably, the limitation of the reference voltage vector magnitude by the edges of a hexagon enables the implementation of overmodulation strategies in the pulsewidth modulator [2]. This permits operation at increased inverter output voltage, thus extending the speed range and improving the dynamic performance.
- Another source of time delay is the pulsewidth modulator. It receives the information $\boldsymbol{u}^*_{s,k+1}$ from the deadbeat

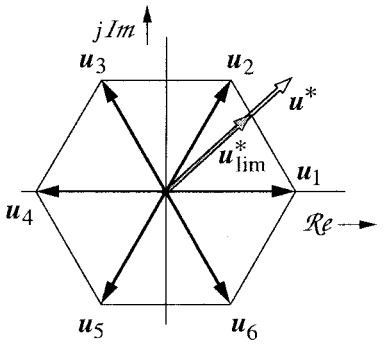

Fig. 7. Nonlinear amplitude limiting of the reference voltage vector in stator coordinates.

controller (14) at sampling instant $k+1$. This information is related to a change of the system state at the earlier sampling instant k. The modulator outputs a sequence of switching states in synchronism to the sampling clock. This sequence controls the average stator voltage during the time interval that terminates at instant $k+2$. The average stator voltage then equals the reference voltage $\boldsymbol{u}^*_{s,k+1}$. Thus, the modulator reference $\boldsymbol{u}^*_{s,k+1}$ has established the desired machine state only at sampling instant $k+2$.

The rotor position angle has advanced during the modulation interval to $\delta_{k+2} = \delta_{k+1} + \omega T_s$; as a consequence, the rotor induced voltage has advanced to $\boldsymbol{u}_{i,k+1} e^{j\omega T_s}$. To adapt the stator voltage to the new angular position, the reference voltage vector of the pulsewidth modulator is rotated by ωT_s, as shown in Fig. 6.

The dynamic performance of a current control system using the predictive deadbeat controller is shown in Fig. 8. The machine operates at rated negative speed in the generator mode, $\omega = -1$; thus, the back EMF adds to the inverter voltage, and saturation of the pulsewidth modulator is avoided. The modulator saturates all the same in the oscillogram in Fig. 8(a), and the commanded current change is not fully reached in one sampling interval. A comparison with the performance of the compensated PI controller shows that, as expressed by the sampled data waveforms, the response time is reduced to its minimum value of $2T_s = 200\ \mu$s. The overshoot is eliminated. Note that the real delay time can be only observed when analog waveforms are recorded.

A remaining problem is the offset in the d-axis current which is caused by a prediction error.

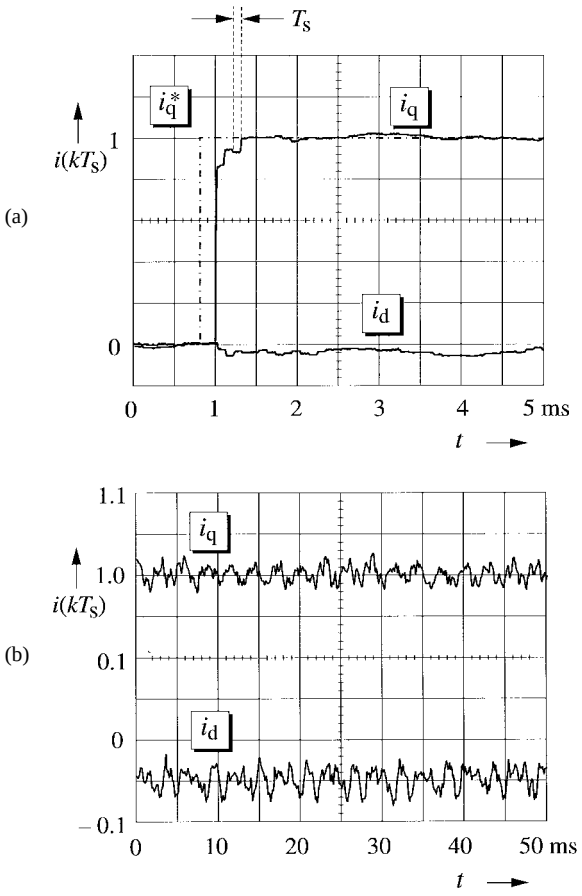

Fig. 8. Performance of the predictive deadbeat controller. (a) Step response at $\omega = -1$. (b) Steady-state operation at rated load.

C. Improved Current Predictor

The signals of the predictive deadbeat current control system described in the previous section represent the respective system variables accurately only at a given sampling instant. The variables are subject to changes during the subsequent time interval. The changes are particularly high when a step command is applied to the system. The consequence is a prediction error.

The situation is improved when the system state is represented by predicted average values of the system variables. The average is taken over a sampling time integral T_s. The predictor equation (13) becomes

$$\hat{\boldsymbol{i}}_{s,k+1} = \boldsymbol{i}_{s,k} + (\boldsymbol{u}^*_s - r_s \bar{\boldsymbol{i}}_{s,k} - \overline{\boldsymbol{u}}_i(\delta) - j\omega \boldsymbol{l}_s * \bar{\boldsymbol{i}}_{s,k}) T_s * \boldsymbol{l}_s^{-1}. \tag{16}$$

Here, the average stator current $\bar{\boldsymbol{i}}_{s,k} = (\boldsymbol{i}_{s,k} + \boldsymbol{i}_{s,k+1})/2$ is difficult to compute, as $\boldsymbol{i}_{s,k+1}$ is not known at the sampling instant k. It can be replaced by $\boldsymbol{i}^*_k$ on the assumption that the deadbeat algorithm will eliminate the current error at the end of any sampling interval. This assumption is true unless a large-signal input change is commanded at higher speed, owing to which the pulsewidth modulator might saturate.

The average value $\overline{\boldsymbol{u}}_i(\delta)$ is approximated as $\boldsymbol{u}_i(\delta + 0.5\omega T_s)$. The approximation is fairly accurate when $\boldsymbol{u}_i(\delta)$ changes monotonously; there will be errors when $\boldsymbol{u}_i(\delta)$ assumes a maximum or a minimum value. This happens quite frequently, owing to the harmonic content of the rotor induced voltage (7). The approximation error increases as ω increases, reaching its maximum value of ≈0.5% at rated speed, which is acceptable.

Since the mechanical speed ω does not change much during a sampling period, the sampled value ω_k is considered to equal its average. Finally, owing to the operating principle of the pulsewidth modulator, its reference voltage $\boldsymbol{u}^*_s$ inherently equals the average stator voltage $\overline{\boldsymbol{u}}_s$ of the subsequent sampling interval.

D. The Deadbeat Current Controller

The foregoing considerations that have improved the current predictor apply to the deadbeat current controller as well. Thus, its algorithm is also modified, replacing the sampled values in (14) by their predicted average values in the subsequent time interval:

$$\boldsymbol{u}^*_{s,k+1} = r_s \hat{\bar{\boldsymbol{i}}}_{s,k+1} + \boldsymbol{l}_s * \frac{\boldsymbol{i}^*_{s,k} - \hat{\boldsymbol{i}}_{s,k+1}}{T_s} + j\omega_k \boldsymbol{l}_s * \hat{\bar{\boldsymbol{i}}}_{s,k+1} + \boldsymbol{u}_i(\delta + 1.5\omega T_s). \tag{17}$$

In this equation, the average value $\hat{\bar{\boldsymbol{i}}}_{s,k+1} = (\boldsymbol{i}_{s,k+1} + \boldsymbol{i}_{s,k+2})/2$ is approximated by

$$\hat{\bar{\boldsymbol{i}}}_{s,k+1} = \frac{\hat{\boldsymbol{i}}_{s,k+1} + \boldsymbol{i}^*_{s,k+1}}{2} \tag{18}$$

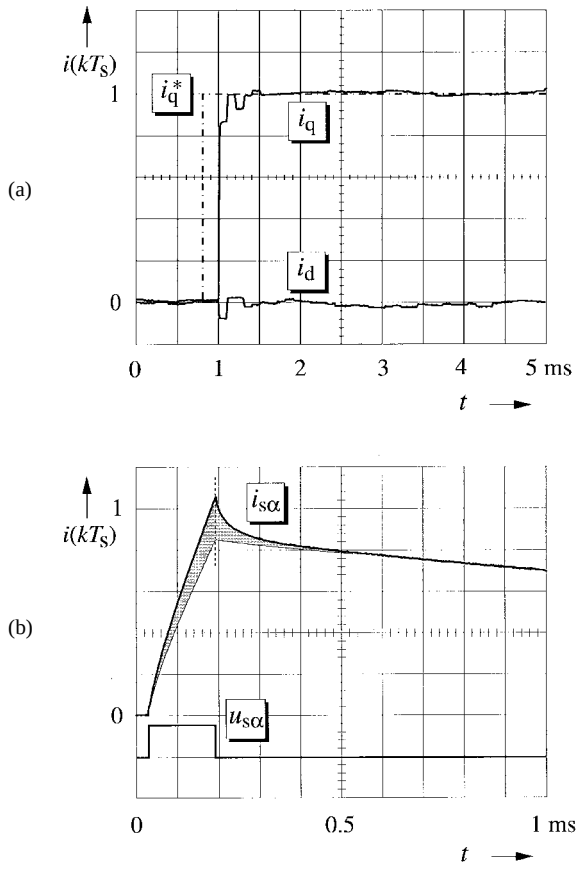

Fig. 9. Performance of the improved predictive deadbeat controller. (a) Step response at $\omega = -1$. (b) Influence of eddy currents in the stator iron on the stator current waveform at a large current step change.

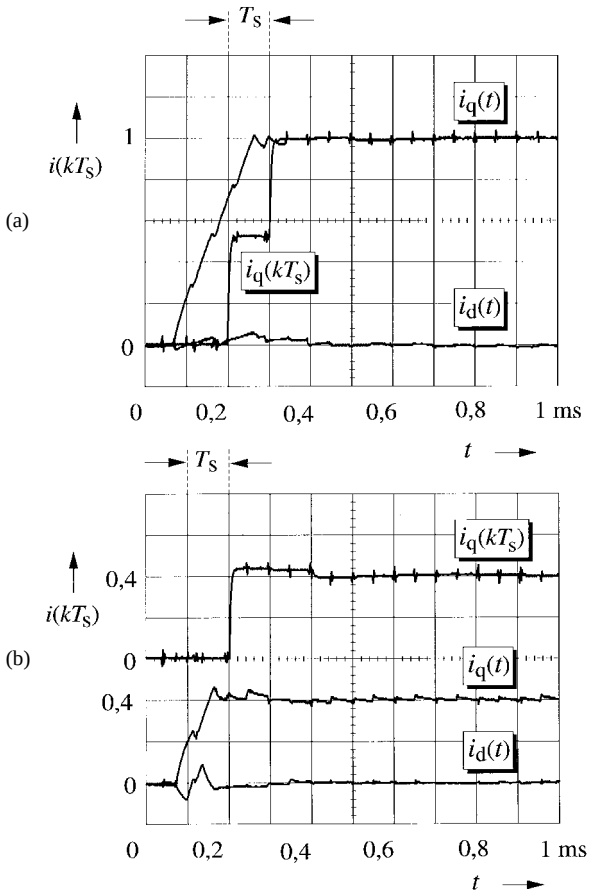

Fig. 10. Predictive deadbeat controller with eddy-current compensation. Comparison of the internal microcontroller signals with the exact current waveforms. (a) Large-signal step response at regeneration, $\omega = -1$. (b) Small-signal step response.

given that $\boldsymbol{i}_{s,k+2}$ is difficult to predict. Substituting the earlier reference value instead gives at least acceptable results at large-signal changes. The average rotor induced voltage $\overline{\boldsymbol{u}}_{i,k+1}$ in (17) is approximated by

$$\overline{\boldsymbol{u}}_i(\delta)_{k+1} = \omega(j\psi_{sf}(\delta)e^{1.5\omega T_s} + \Phi(\delta + 1.5\omega T_s)) \qquad (19)$$

which is in agreement with the considerations of the previous section. The average value $(\boldsymbol{u}(\delta)_{k+1} + \boldsymbol{u}(\delta)_{k+2})/2$ is obtained by addressing the table at an added lead angle $\omega T_s/2$, such that the total lead angle is $1.5\omega T_s$.

The response of the improved predictive deadbeat controller to a high-amplitude step change is shown in Fig. 9(a). The q-axis current reaches its maximum value after the unavoidable two sampling periods; the full commanded value is not reached in a single step as the modulator saturates.

An undershoot of about 5% occurs in the i_q waveform before zero error is obtained for both current components. The reason for this is eddy currents in the stator iron that are generated at large-signal current changes. This is exemplified in the response Fig. 9(b) of the stator current to a single voltage pulse. The pulse duration is chosen such that the current builds up to its rated value. The subsequent decay is determined by the voltage drop of the inverter diodes and the stator resistance. Superimposed to that is a dynamic eddy-current component that builds up during the pulse and then rapidly decays; the time constant is 30 μs. The amplitude of the eddy-current pulse is almost proportional to the rate of current change in a transient condition. Moreover, an eddy-current pulse occurs predominantly in the q-axis, as the d-axis current is normally held at zero.

The unmodeled eddy currents increase the total current to more than its predicted value; the controller then commands a reduced value in the next step.

To define an eddy-current compensation signal, the current slope for the sampling integral k is determined by the difference of the sampled current $\boldsymbol{i}_{s,k}$ and the predicted current $\hat{\boldsymbol{i}}_{s,k+1}$. This leads to

$$\boldsymbol{u}_{e,k+1} = \boldsymbol{u}^*_{e,k+1} + \boldsymbol{k}_e(\hat{\boldsymbol{i}}_{s,k+1} - \boldsymbol{i}_{s,k}), \qquad \boldsymbol{k}_e = k_e + j0. \quad (20)$$

The parameter k_e is determined by experiment. The implementation is shown in Fig. 6 where it is marked by a shaded area.

E. Performance

Step response waveforms with eddy-current compensation are presented in Fig. 10(a) for large-signal excitation and in Fig. 10(b) for small-signal excitation. In addition to the sam-

pled current waveforms $\boldsymbol{i}(kT_s)$, the measured analog waveforms $\boldsymbol{i}(t)$ are displayed. Note that the waveforms appear delayed in all other oscillograms of this paper, since it is always sampled data that are displayed. It can be observed in Fig. 10 that the large-signal response results are slightly undercompensated, and the small-signal response slightly overcompensated. The current ripple is now negligible.

The bandwidth of the deadbeat current control system was measured at sinusoidal excitation; it was found as 3.5 kHz at 3-dB amplitude reduction. The upper frequency limit for the particular purpose of torque-ripple compensation is still higher, provided the parasitic effects of the machine are accurately modeled. The model [7] that is implemented here makes the torque ripple fully predictable. Hence, the compensation current is generated without delay; it is exactly in antiphase to the torque ripple of the machine. The bandwidth limit for the compensation is then determined only by the switching frequency.

An accurate model of the parasitic effects of the machine that has self-learning and self-adjusting properties is described in [7]. This article also reports on the performance of torque-ripple compensation.

The complete pulsewidth modulation, deadbeat current control, and torque-ripple compensation scheme, including the self-adjusting model, is implemented in a low-cost microcontroller 80C166. It is this low-cost approach that limits the sampling frequency to 10 kHz. The switching frequency is 10 kHz, with one sampling clock cycle controlling two modulation half cycles having identical switching patterns. This clearly compromises on bandwidth, which could be doubled if a faster microcontroller was used at 20-kHz clock cycle.

The predictive deadbeat controller is designed with a view to compensate the high-frequency torque ripple of a PM synchronous machine drive. It can be used, of course, in a simplified structure to implement high-bandwidth current control in any other high-performance drive.

V. Summary

A predictive deadbeat current control system has been designed to compensate the inherent sampling delay of digital signal processing hardware to the extent possible. Accurate deadbeat current response is achieved, even with PM machines that generate parasitic high-frequency current components owing to unavoidable harmonics in flux linkage distribution. The quality of the current waveforms is that much improved that another parasitic effect becomes observable: eddy currents in the laminated stator iron produce a 30-μs current pulse whenever a steeper current rise is commanded. The pulses can be eliminated, if desired, by a simple compensation scheme. The 3-dB bandwidth was measured as 3.5 kHz at 10-kHz switching frequency. Torque-ripple compensation is possible at even higher frequencies, since an accurate model of the parasitic effects of the PM motor renders the system deterministic. In a simpler structure, the deadbeat current controller is suited to implement high-bandwidth current control in any other high-performance drive.

Appendix

The data for the eight-pole PM machine are as follows:

rated power	1700 W
rated speed	3000 r/min
rated current	6.8 A
rated torque @ 100 °C	5.6 N·m
rated back EMF	148 V
d-axis inductance	3.1 mH
number of poles	8
maximum speed	6000 r/min
maximum current	64 A
maximum torque	52 N·m
stator resistance	0.9 Ω
q-axis inductance	3.4 mH.

References

[1] G. Pfaff, A. Weschta, and A. Wick, "Design and experimental results of a brushless AC servo drive," in *Conf. Rec. IEEE-IAS Annu. Meeting*, San Francisco, CA, 1982, pp. 692–697.

[2] J. Holtz, W. Lotzkat, and A. Khambadkone, "On continuous control of PWM inverters in the overmodulation range with transition to the six-step mode," *IEEE Trans. Power Electron.*, vol. 8, pp. 546–553, Oct. 1993.

[3] T. M. Jahns, "Motion control with permanent-magnet AC machines," *Proc. IEEE*, vol. 82, pp. 1241–1252, Aug. 1994.

[4] H. Le Huy, R. Perret, and R. Feuillet, "Minimization of torque ripple in brushless DC motor drives," in *Conf. Rec. IEEE-IAS Annu. Meeting*, Toronto, Ont., Canada, 1985, pp. 790–797.

[5] E. Favre, L. Cardoletti, and M. Jufer, "Permanent-magnet synchronous motors: A comprehensive approach to cogging torque suppression," *IEEE Trans. Ind. Applicat.*, vol. 29, pp. 1141–1149, Nov./Dec 1993.

[6] B.-J. Brunsbach, G. Henneberger, and Th. Klepsch, "Compensation of torque ripple," in *Conf. Rec. Electrical Machines and Drives Conf.*, Oxford, U.K., 1993, pp. 588–593.

[7] J. Holtz and L. Springob, "Identification and compensation of torque ripple in high-precision permanently magnet motor drives," *IEEE Trans. Ind. Electron.*, vol. 43, pp. 309–320, Apr. 1996.

[8] J. Holtz, "The representation of AC machine dynamics by complex signal flow graphs," *IEEE Trans. Ind. Electron.*, vol. 42, pp. 263–271, June 1995.

[9] ——, "Pulsewidth modulation—A survey," *IEEE Trans. Ind. Electron.*, vol. 39, pp. 410–420, Oct. 1992.

[10] ——, "Methods for speed sensorless control of AC drives," in K. Rajashekara, Eds., *Sensorless Control of AC Motors*. Piscataway, NJ: IEEE Press, 1996.

[11] Y. Murai, T. Watanabe, and H. Iwaski, "Waveform distortion correction circuit for PWM inverters with switching lag-times," *IEEE Trans. Ind. Applicat.*, vol. 23, pp. 881–886, 1987.

Lothar Springob received the Dipl.-Ing. degree from the University of Bochum, Bochum, Germany, and the Dr.-Ing. degree from Wuppertal University, Wuppertal, Germany, in 1987 and 1994, respectively.

In 1987, he joined the Electrical Machines and Drives Laboratory, University of Wuppertal, as a Research Assistant. Since 1994, he has been with Vectron Elektronik GmbH, Krefeld, Germany. His interests relate to problems of ac machines and drive control.

Joachim Holtz (M'87–SM'88–F'93) graduated in 1967 and received the Ph.D. degree in 1969 from the Technical University Braunschweig, Braunschweig, Germany.

In 1969, he joined the Indian Institute of Technology, Madras, India, as an Associate Professor, and became a Full Professor and Head of the Control Engineering Laboratory in 1971. He joined the Siemens Research Laboratories, Erlangen, Germany, in 1972. Since 1976, he has been Professor and Head of the Electrical Machines and Drives Laboratory, Wuppertal University, Wuppertal, Germany. He is the author of more than 100 technical papers. He is the coauthor of four books and the holder of 27 patents.

Dr. Holtz is a recipient of the Dr. Eugene Mittelmann Achievement Award from the IEEE Industrial Electronics Society, the Outstanding Achievement Award from the IEEE Industry Applications Society, and the William E. Newell Award from the IEEE Power Electronics Society. He has earned four IEEE Prize Paper Awards. He is a Distinguished Lecturer of the IEEE Industry Applications and IEEE Industrial Electronics Societies. He is Editor-in-Chief of the IEEE TRANSACTIONS ON INDUSTRIAL ELECTRONICS and a member of the Administration Committee of the IEEE Industrial Electronics Society. He is also a member of the Static Power Converter Committee of the IEEE Industry Applications Society and the German professional organizations, VDE and GMA.